

Fig. 1. A schematic diagram of a Ni-MH cell and the model representation

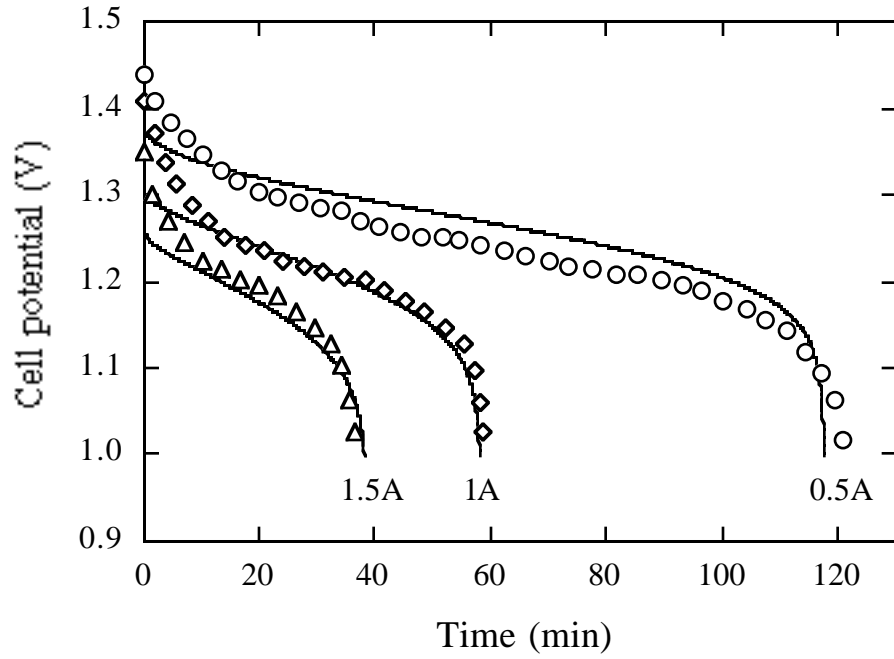
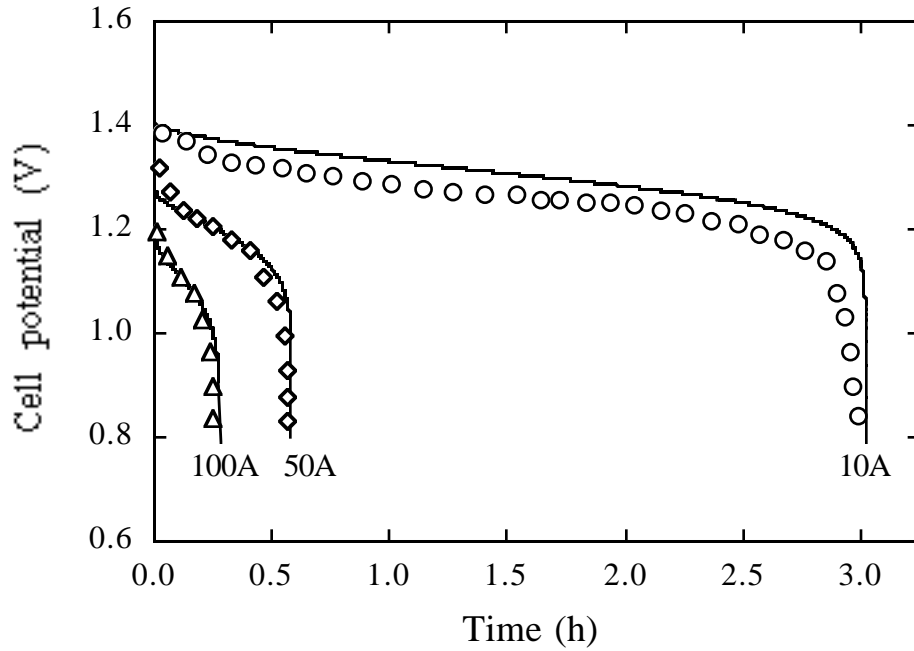
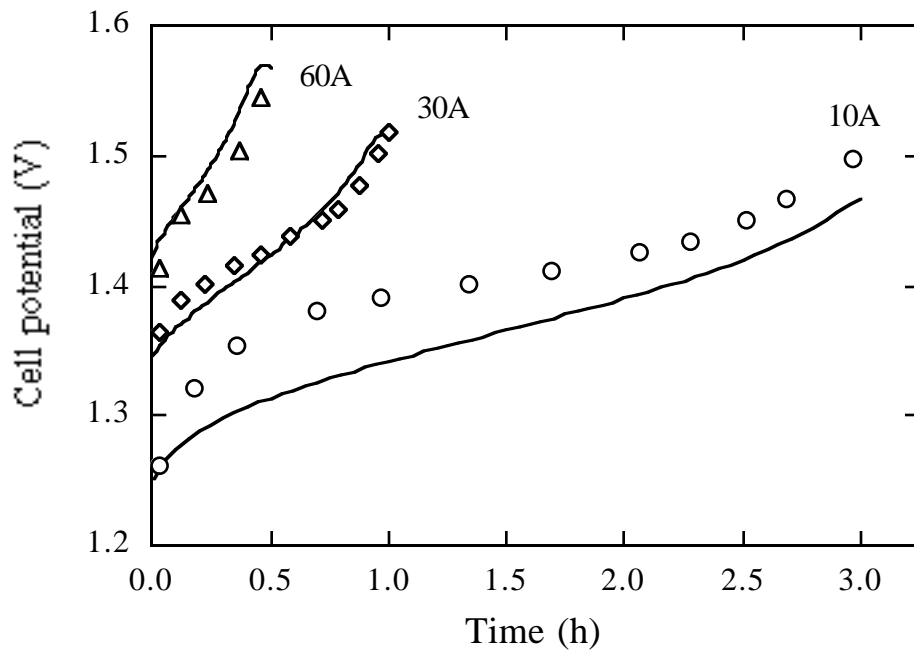


Fig. 2. Comparison of predicted cell discharge potential (solid lines) with experimental results (symbols)



(a)



(b)

Fig. 3. Comparison of predicted cell potentials (solid lines) with the experimental results from the literature (symbols, Sakai et al, 1991): (a) discharge and (b) charge

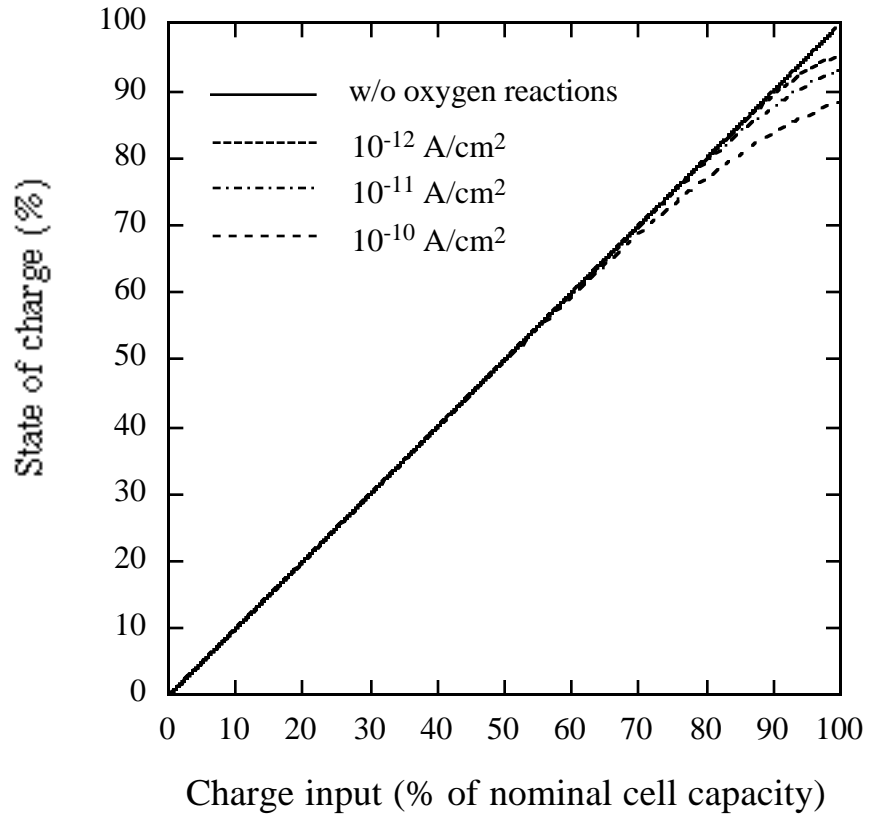
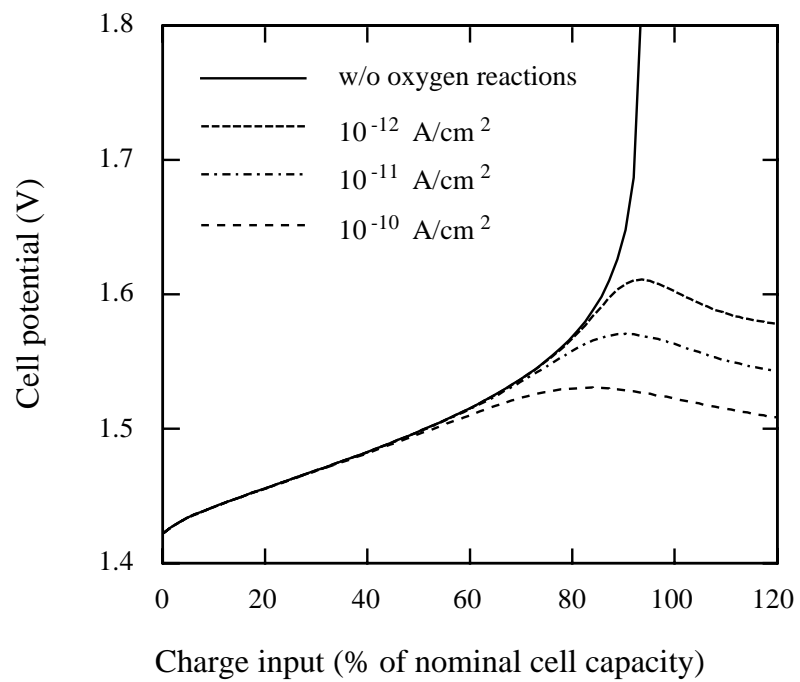
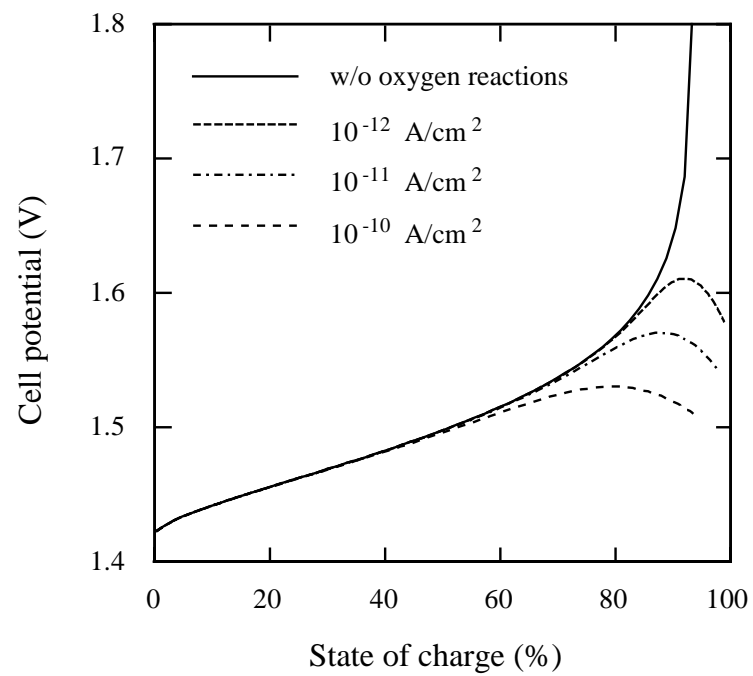


Fig. 4. State of charge of the Ni-MH cell during 2C charging at various exchange current densities of the oxygen generation reaction



(a)



(b)

Fig. 5. Cell potential curves of the Ni-MH cell during 2C charging at various exchange current densities of the oxygen generation reaction: (a) cell potential vs. charge input and (b) cell potential vs. state of charge

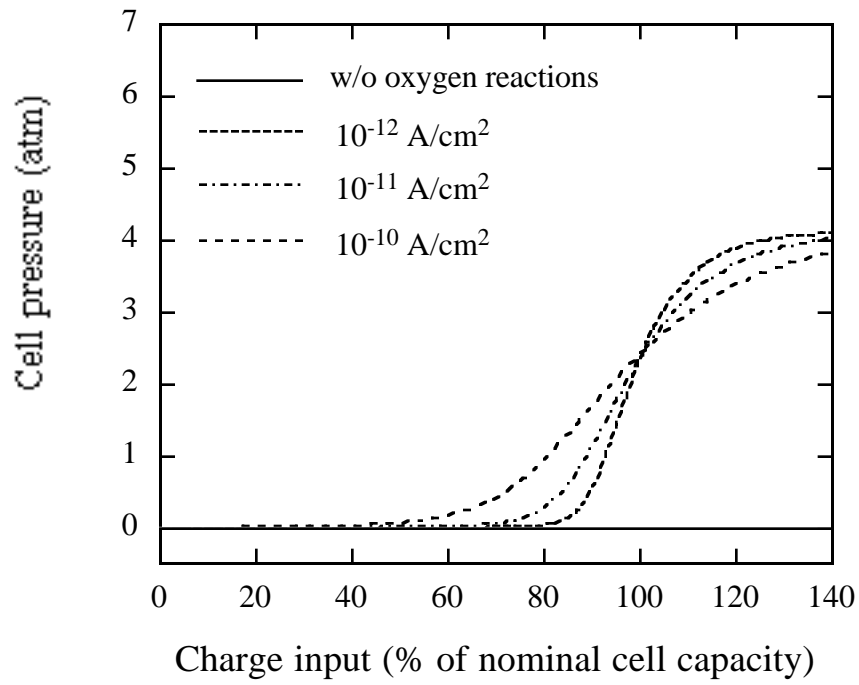
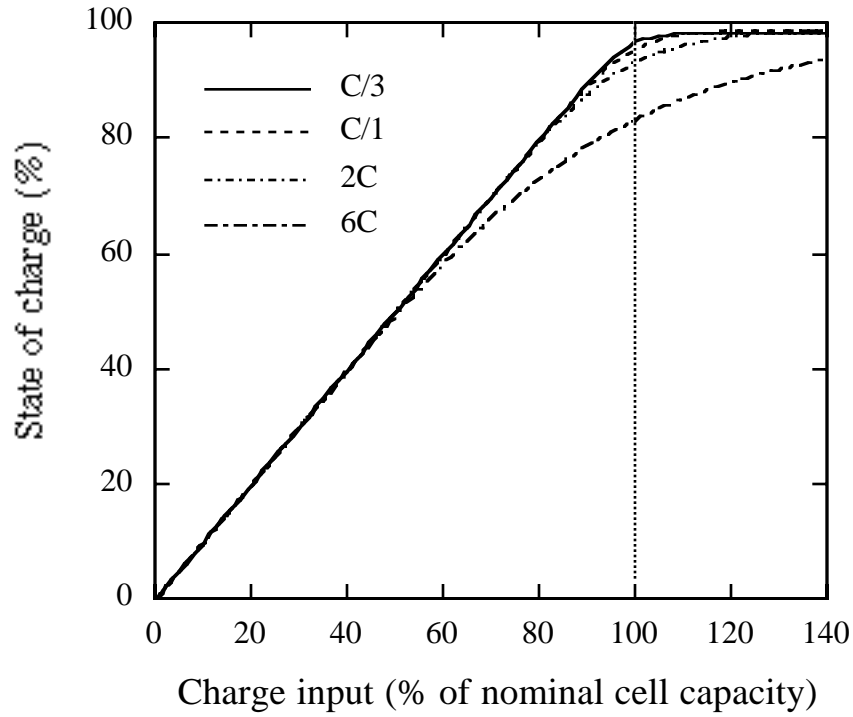
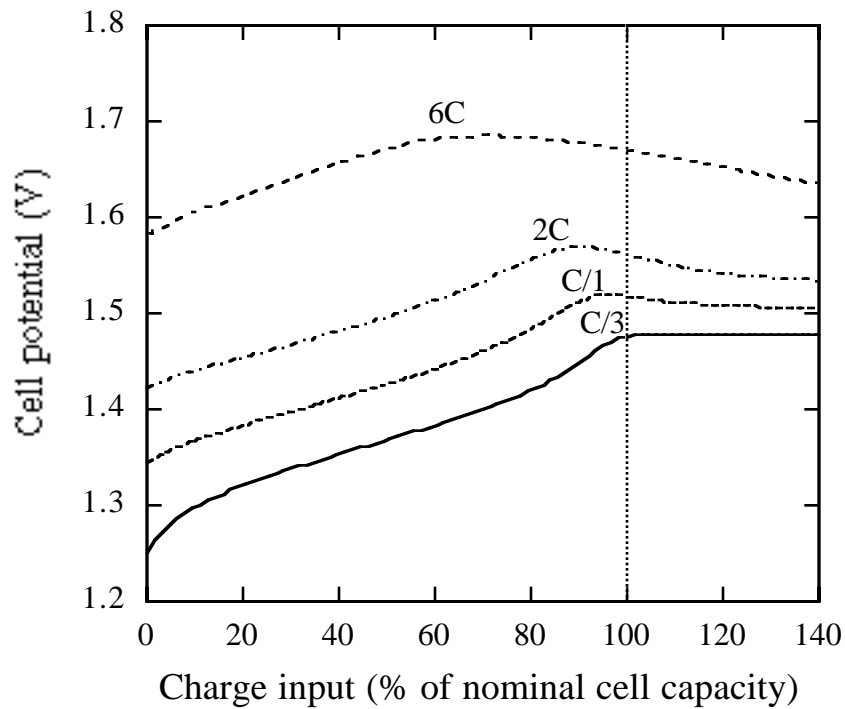


Fig. 6. Cell pressure profiles during 2C charging at various exchange current densities of the oxygen generation reaction



(a)



(b)

Fig. 7. Effect of oxygen evolution on the behavior of the Ni-MH Cell at various charge rates: (a) State of charge vs. charge input percentage of nominal cell capacity; and (b) cell potential vs. state of charge

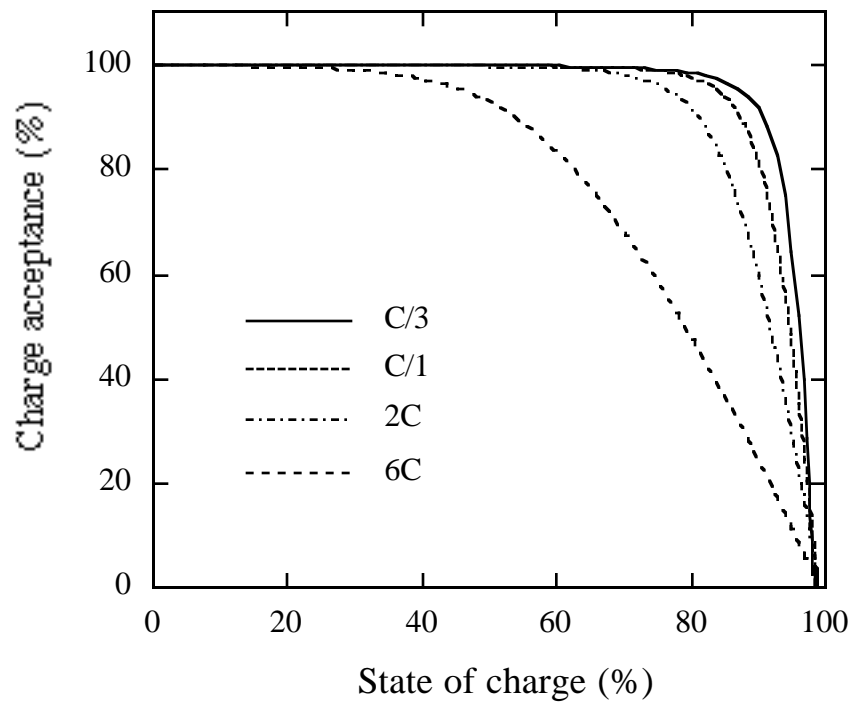


Fig. 8. Charge acceptance vs. state of charge of the Ni-MH cell at various charging rates as a result of oxygen reactions

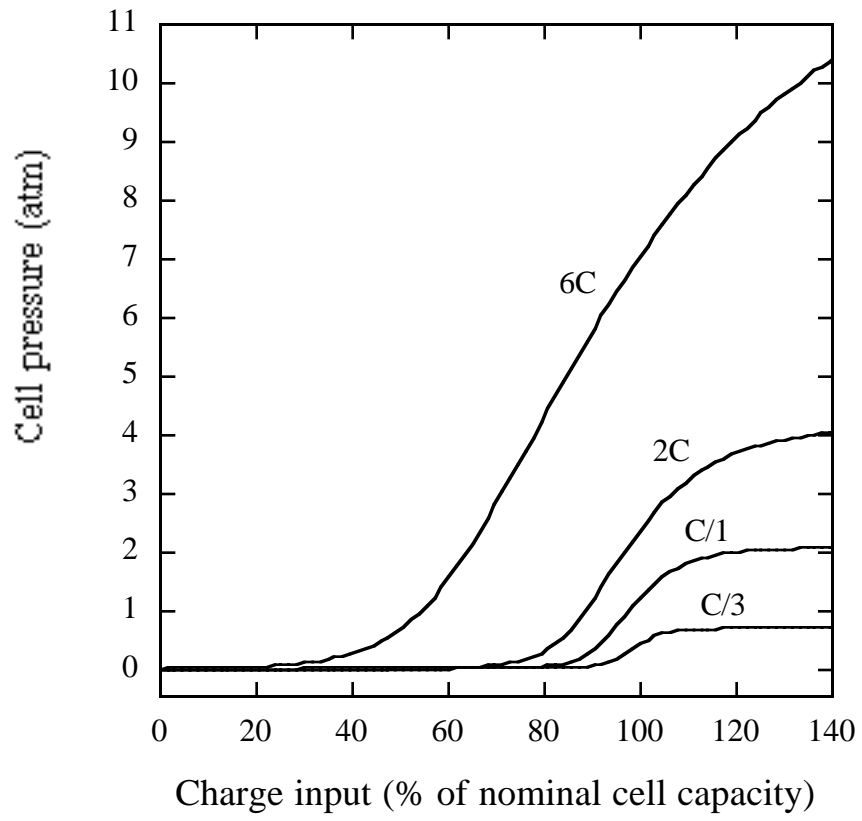


Fig. 9. Cell pressure profiles of the Ni-MH cell at various charging rates

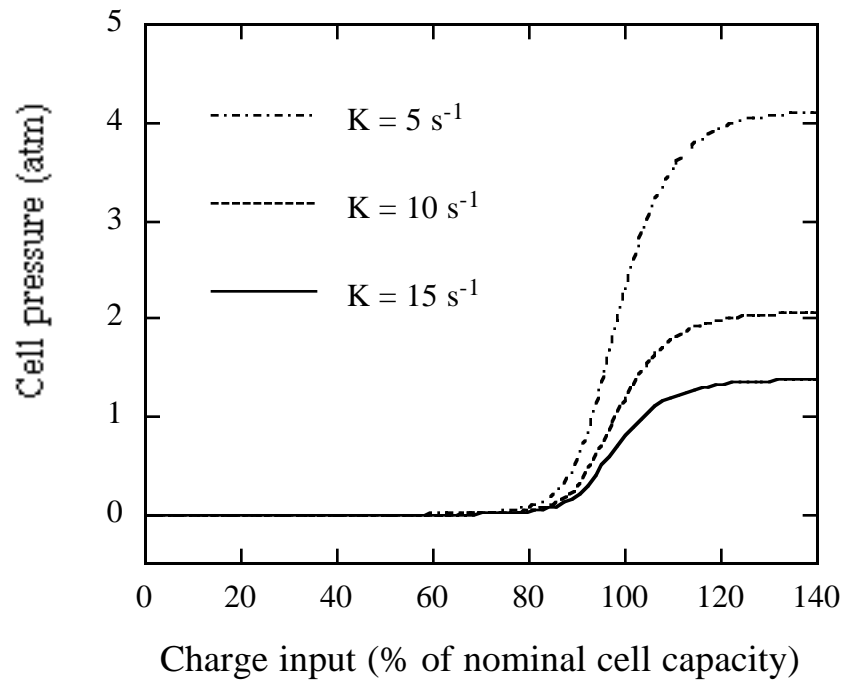


Fig. 10. Effect of the interfacial mass transfer coefficient on the cell pressure variation during C/1 charging

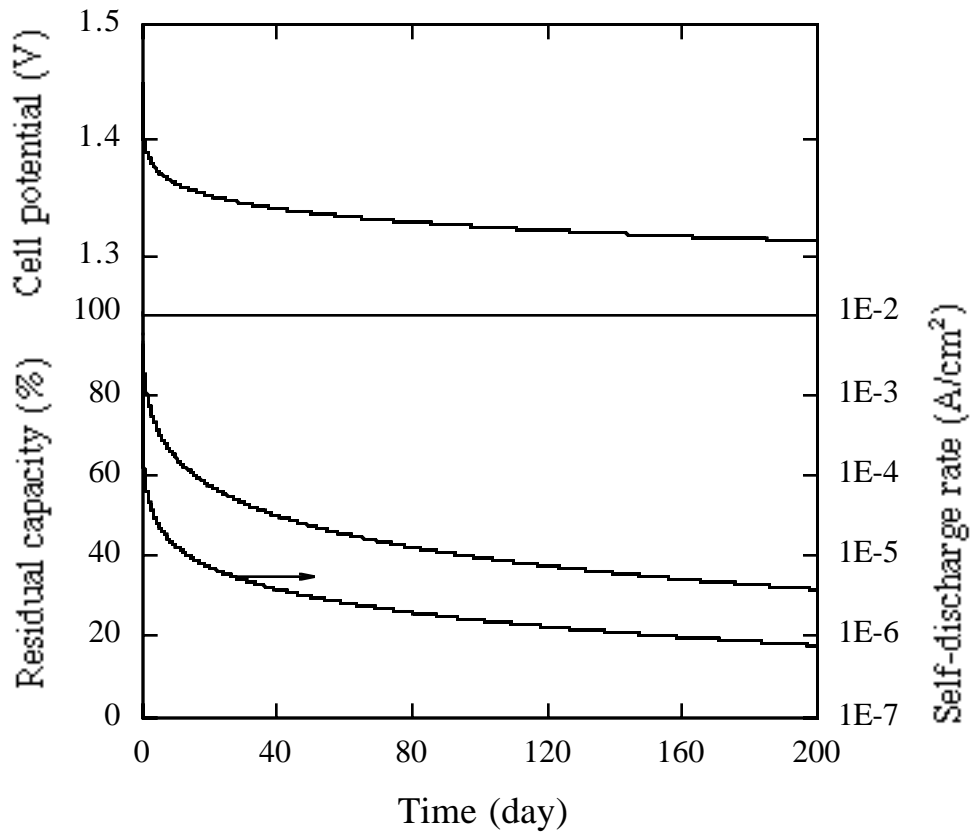


Fig. 11. Cell potential, self-discharge rate, and residual capacity vs. time curves of the Ni-MH cell as a result of oxygen reactions

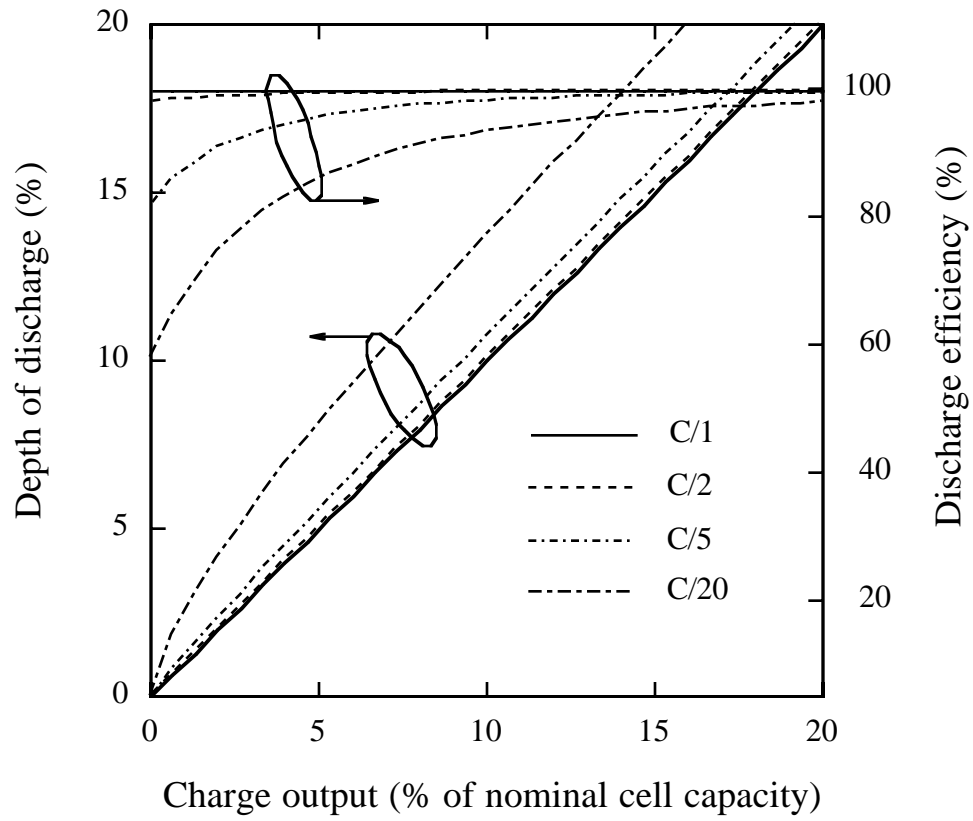


Fig. 12. Effect of oxygen evolution on the discharge efficiency and depth of discharge of the Ni-MH cell at various rates

-----